

REVIEW ARTICLE

# Fluorescent Pteridine Nucleoside Analogs

## *A Window on DNA Interactions*

**Mary E. Hawkins**

*Pediatric Oncology Branch, National Cancer Institute, Bethesda, MD 20892*

*Email: mh100x@nih.gov*

### Abstract

Pteridine nucleoside analog probes are highly fluorescent and offer different approaches to monitor subtle DNA interactions with other molecules. Similarities in structure and size to native nucleosides make it possible to incorporate these probes into oligonucleotides through the standard deoxyribose linkage. These probes are formulated as phosphoramidites and incorporated into oligonucleotides using automated DNA synthesis. Their position within the oligonucleotide renders them exquisitely sensitive to changes in structure as the oligonucleotide meets and reacts with other molecules. Changes are measured through fluorescence intensity, anisotropy, lifetimes, spectral shifts, and energy transfer. The fluorescence properties of pteridine nucleoside analogs as monomers and incorporated into single and double stranded oligonucleotides are reviewed. The two guanosine analogs, 3MI and 6MI, and two adenosine analogs, 6MAP and DMAP, are reviewed in detail along with applications utilizing them.

### INTRODUCTION

Pteridines are naturally occurring, highly fluorescent compounds that were first isolated from butterfly wings in 1889. There is an extensive literature on the subject of these molecules most of which is concerned with the organic synthesis of various derivatives or clinical formulations used in the treatment of cancer and other diseases.

This Article will concentrate on pteridines used as nucleoside analogs incorporated into DNA. The development of pteridines for DNA applications has focused on those compounds that are similar in structure to native nucleosides, are stable enough to withstand the caustic treatment used in automated DNA syn-

thesis and are highly fluorescent (1,2). Structurally similar to native nucleosides, the pteridines described here are incorporated into DNA through a deoxyribose moiety identical to that of native DNA with no "linker-arm" attachment involved.

Because of this native-like linkage to DNA, these probes are very closely associated with neighboring bases rendering them exquisitely sensitive to subtle changes that occur in the DNA structure surrounding them. Changes in base stacking or base pairing in the vicinity of these probes are reflected by distinct changes in the fluorescence properties of the pteridine.

This sensitivity to neighboring bases is not duplicated by conventional linker-attached

probes which are more removed from these interactions by the length of the carbon chain connecting them to the DNA. Probes which are dissimilar to nucleosides in size and structure cannot be linked to the DNA through a deoxyribose moiety without a linker because they would most likely disrupt the DNA tertiary structure and therefore not allow native-like interactions. Placement of these bulky probes on extended linkers allows their use without disruption of DNA interactions at the cost of distancing them from the site of interest.

The use of a deoxyribose linkage confers another advantage besides the proximity to events of interest. Conventional, linker-attached probes can allow independent movement of the fluorophore leading to more complex results that can be difficult to interpret. Because of the relationship between fluorescence quenching of the pteridine probes and the identity of neighboring bases, it is logical to assume that the probes are somewhat involved in base stacking. This environment should greatly limit the independent movement of the probe. Anisotropy results using pteridine analogs have supported this hypothesis (2a).

Another feature of these probes that can be used to advantage is that they are quenched when incorporated into an oligonucleotide (sometimes referred to as self-quenching). While at first this quenching may not seem to be advantageous, this feature can be used in many ways to monitor changes in tertiary structure occurring within the DNA as the bases interact with other molecules. Because most of the quench experienced by the pteridine probes in an oligonucleotide is due to base stacking interactions, events that affect base stacking are reflected directly by changes in fluorescence properties. It has been demonstrated experimentally that disruptions in the tertiary structure of DNA can clearly be monitored through changes in fluorescence intensity using the pteridine nucleoside analogs (1–3). In many cases, when using the nucleoside analog probes, the products of a reaction do not need to be separated prior to analysis, a distinct advantage over other methods.

These probes also have a favorable spectral position, with absorption near 350 nm which overlaps well with the emission spectrum of tryptophan. In a fluorescence resonance energy transfer system, tryptophan, which emits near 350 nm would be the donor and these fluorophores could serve as acceptors, if within ~30 Angstroms of the tryptophan (4). In a trp containing protein that binds DNA, this would allow one to map the binding with respect to the tryptophan.

In the following pages, the fluorescence properties of pteridine nucleoside analogs are described first as monomers and then as they are incorporated into single and double stranded oligonucleotides. This is followed by descriptions of applications utilizing these analogs.

## FLUORESCENCE PROPERTIES OF PTERIDINE NUCLEOSIDE ANALOG MONOMERS

In a search for potential nucleoside analog probes, Hawkins and coworkers (2) first measured the relative quantum yields ( $Q_{rel}$ ) of the 18 ribo- and deoxyribo-pteridine compounds shown in Figure 1. Probes 6, 7–9, and 11–16 (lower portion Fig. 1) were found to have very low  $Q_{rel}$ 's (<0.033) and consequently were not examined further. Probes 1, 2, 4 (3MI), 5, 10, 17 (6MI) and 25 (upper part of Fig. 1) were found to be highly fluorescent and worthy of further consideration. Spectral properties of probes that were investigated further are grouped according to structural similarities in Table 1. The adenosine analogs, (1, 2, and 25) have a 4-amino-7-oxo configuration and only differ by the presence and placement of a phenyl group. Probe 2 (6-phenyl substituted) has the lowest  $Q_{rel}$  and shortest mean lifetime. The guanosine analogs, probes 4 (3MI), 5, and 17 (6MI) (2-amino-4,7-oxo derivatives) differ only by presence and placement of a methyl group. These probes exhibit similar  $Q_{rel}$  (0.70 to 0.88) and species-concentration-weighted lifetimes ( $\tau_m$ ) ranges from 5.63 to 6.54 ns. Probe 10 is the 2-oxo-4-amino-6,7-methyl substituted probe and

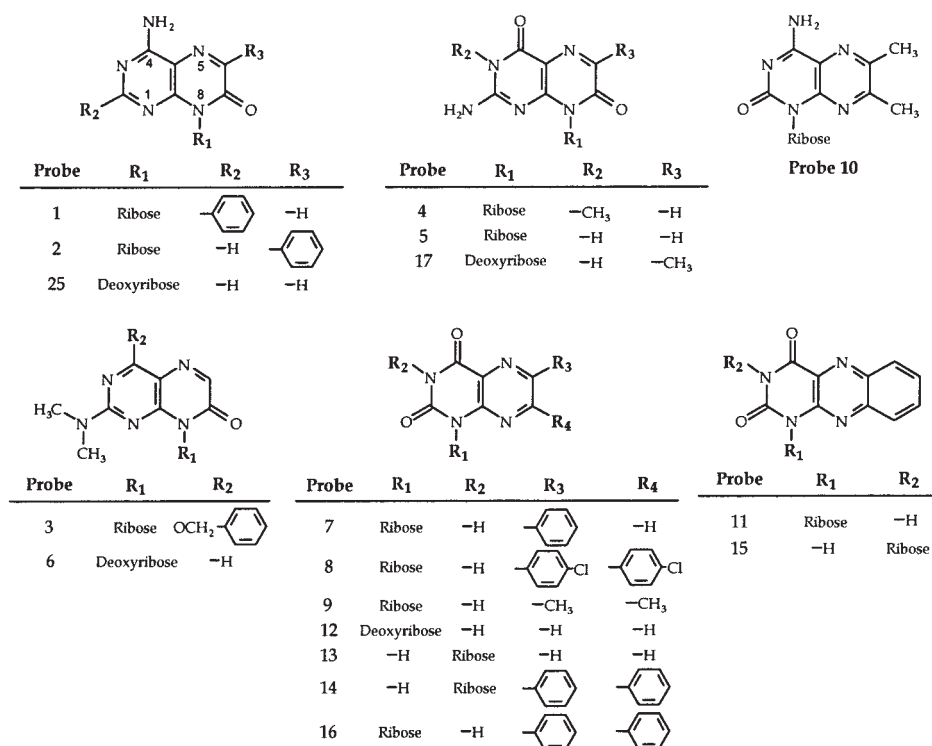


Fig. 1. Chemical structures of the pteridine nucleoside analogs. Compounds are grouped according to similarities in their chemical structures. Reprinted with permission from ref. 1. Probe 4 is also referred to as 3MI and probe 17 is 6MI.

Table 1  
Fluorescence properties of Pteridine Nucleoside Analogs. (Adapted from ref. 1.)

Probe	Ex <sub>max</sub> <sup>a</sup>	Em <sub>max</sub> <sup>b</sup>	Q <sub>rel</sub> <sup>c</sup>	τ <sub>i</sub> (ns) <sup>d</sup>	α <sub>i</sub> <sup>e</sup>	%I <sub>1</sub> <sup>f</sup>	τ <sub>m</sub> <sup>g</sup>	<τ> <sup>h</sup>
1	354	444	0.41	τ <sub>1</sub> =1.91 τ <sub>2</sub> =4.05	α <sub>1</sub> =0.19 α <sub>2</sub> =0.81	I <sub>1</sub> =9.9 I <sub>2</sub> =90.1	3.84	3.64
2	358	440	0.16	τ <sub>1</sub> =0.76 τ <sub>2</sub> =1.05	α <sub>1</sub> =0.67 α <sub>2</sub> =0.33	I <sub>1</sub> =59.6 I <sub>2</sub> =40.4	0.87	0.85
25	334	443	0.27	τ <sub>1</sub> =2.37 τ <sub>2</sub> =4.13	α <sub>1</sub> =0.19 α <sub>2</sub> =0.81	I <sub>1</sub> =11.6 I <sub>2</sub> =88.4	3.92	3.80
4 (3MI)	348	430	0.88	τ <sub>1</sub> =3.54 τ <sub>2</sub> =6.58	α <sub>1</sub> =0.02 α <sub>2</sub> =0.98	I <sub>1</sub> =1.2 I <sub>2</sub> =98.8	6.54	6.51
5	348	430	0.87	τ <sub>1</sub> =1.81 τ <sub>2</sub> =6.26	α <sub>1</sub> =0.37 α <sub>2</sub> =0.63	I <sub>1</sub> =14.6 I <sub>2</sub> =85.4	5.63	4.65
17 (6MI)	340	431	0.70	τ <sub>1</sub> =5.45 τ <sub>2</sub> =6.58	α <sub>1</sub> =0.20 α <sub>2</sub> =0.80	I <sub>1</sub> =17.5 I <sub>2</sub> =82.5	6.38	6.35
10	336	400	0.54	τ <sub>1</sub> =3.16 τ <sub>2</sub> =8.14	α <sub>1</sub> =0.97 α <sub>2</sub> =0.03	I <sub>1</sub> =92.8 I <sub>2</sub> =7.2	3.52	3.31

<sup>a</sup>Excitation maximum; <sup>b</sup>Emission maximum; <sup>c</sup>Relative quantum yield; <sup>d</sup>lifetime for each component of a multi-exponential model; <sup>e</sup>pre-exponential for each component of a multi-exponential model; <sup>f</sup>percent fluorescence intensity for each component of a multi-exponential model; <sup>g</sup>species-concentration-weighted lifetime; <sup>h</sup>intensity-weighted lifetime.

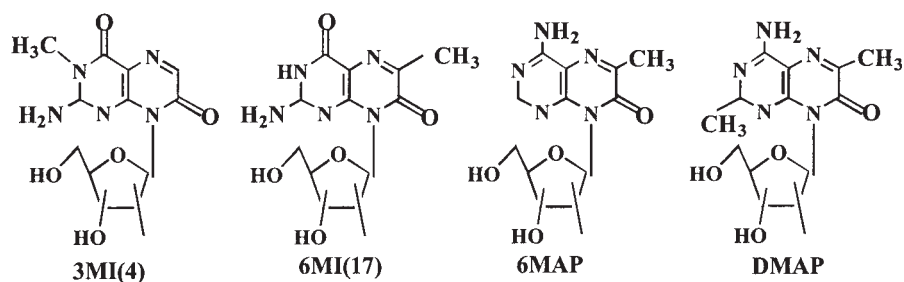


Fig. 2. Four analogs developed for incorporation into oligonucleotides. 3MI (probe 4) and 6MI (Probe 17) are the two guanosine analogs. 6MAP and DMAP are the two adenosine analogs.

it has a  $Q_{rel}$  of 0.54 and a  $\tau_m$  of 3.52 ns. Table 1 lists the fluorescence properties for these compounds. From the group that were initially evaluated, probes 4 (3MI) and 17 (6MI) were chosen for further study.

Changes in pH from 5.0 to 8.0 had no measurable effect on the emission spectrum of 3MI, but the emission spectrum of 6MI was shifted 10 nm to the red when the pH was increased from 7.0 to 8.0. A pH titration of DAS (decay associated spectra) for these two probes revealed that the lifetime components for 3MI also remained unchanged over the pH range from 7.0 to 9.0, while lifetime components for 6MI underwent a blue shift in the longest lived DAS and a smaller increase in the shorter lived component (1). These DAS demonstrate a pH dependent equilibrium between a minimum of 2 emitting species.

Driscoll and others (5) have studied the fluorescence of 3MI monomer in solution. In steady-state and time-resolved fluorescence quenching studies using acrylamide to evaluate the accessibility of solvent to 3MI, their measurements indicate that acrylamide and 3MI form a ground-state complex as evidenced by static quenching. They also observed that there is very little dynamic quenching as demonstrated by a  $k_q$  of  $1 \times 10^8 \text{ M}^{-1} \text{ s}^{-1}$ , an order of magnitude less than that expected for small, well solvated molecules. In other experiments, Driscoll and others compared the steady state and time-resolved fluorescence characteristics of 3MI and 3,8-dimethylisoxanthopterin (DMI), a pteridine compound identical to 3MI

except for a methyl group in place of the deoxyribose moiety. Because the results for both of these compounds were similar, they concluded that the ribose ring probably does not shield the isoxanthopterin ring from dynamic interactions with solutes. In the same study, Driscoll et al observed that the anisotropy decay of 3MI monomer in buffer could be described by a single rotational correlation time near 80 ps. Modeling studies using the HYDRO program (6) suggest that this rotational correlation time is reasonable for 3MI hydrogen bonded to four water molecules.

Two pteridine-based adenosine analogs, 4-amino-8-(2-deoxy- $\beta$ -D-ribofuranosyl)5'-O-dimethoxy-trityl-6-methyl-7 (8H)-pteridone (6MAP) and 4-amino-8-(2-deoxy- $\beta$ -D-ribofuranosyl)5'-O-dimethoxy-trityl,-2,6-dimethyl-7 (8H)-pteridone (DMAP) have recently been developed. (M. Hawkins, et al. submitted) The chemical structures of these probes are shown in Figure 2. Probe 25 (equivalent to 6MAP without the methyl group) was evaluated in the first study (Fig. 2 in ref. 1) and initially seemed to be an ideal fluorescent adenosine analog but was found to be quite unstable. Other potential adenosine analogs, probes 1 and 2 (equivalent to 6MAP and DMAP with phenyl groups in place of the methyl groups) (Fig. 2) (1) were more stable than probe 25, however, the phenyl groups present on these two analogs exhibited a strong quenching effect and due to their size and structure were not ideally suited for our purposes. 6MAP and DMAP were developed by substituting methyl

Table 2  
 Oligonucleotide sequences with 3MI substituting for G (2).

		<sup>a</sup> Q <sub>rel</sub>
PTR1	5 -GTFTGGAAAATCTCTAGCAGT-3	0.13
PTR2	5 -GTGTFGAAAATCTCTAGCAGT-3	0.10
PTR3	5 -GTGTGFAAAATCTCTAGCAGT-3	0.03
PTR4	5 -GTGTGGAAAATCTCTAFCAGT-3	0.06
PTR5	5 -GTGTGGAAAATCTCTAGCAFT-3	0.14
PTR7	5 -CACACCTTTTAFAGATCGTCA-3	0.04
PTR8	5 -CACACCTTTTAGAFATCGTCA-3	0.05
PTR9	5 -CACACCTTTTAGAGATCFTCA-3	0.29

<sup>a</sup>Relative quantum yield.

groups for the phenyl groups present in probes 1 and 2. The methyl moieties stabilize these compounds without the steric and quenching problems associated with the phenyl groups of probes 1 and 2. Because 6MAP is structurally identical to probe 2 (1) except for the substitution of a methyl group for a phenyl group in the 6-position, a comparison of the Q<sub>rel</sub>'s between probe 2 (0.16) and 6MAP(0.38) reveals the quenching effect associated with the phenyl moiety as compared to that of the methyl moiety.

The two adenosine analogs, 6MAP and DMAP showed no detectable degradation (as measured through loss of fluorescence intensity in their emission scans) after exposure to ambient light and room temperature for > 24 hours. Relative quantum yields for 6MAP and DMAP are 0.39 and 0.48 with excitation maxima of 310 and 330 nm respectively and emission maxima at 430 nm. Fluorescence decay curves of both probes are mono-exponential exhibiting lifetimes of 3.8 and 4.8 ns for 6MAP and DMAP respectively.

The four probes that have been incorporated into oligonucleotides are 3MI, 6MI, 6MAP and DMAP. The others have not been pursued for reasons of instability (probes 5 and 25), unfavorable structure (probes 1 and 2) or complications in the DNA synthesis (probe 10). The synthetic method for 3MI is published in Hawkins 1995 (2). The following

section will describe the fluorescence properties of these four analogs as they are incorporated into oligonucleotide single and double strands.

### FLUORESCENCE PROPERTIES OF PTERIDINE NUCLEOSIDE ANALOG-CONTAINING OLIGONUCLEOTIDES

All four of the pteridine analogs, 3MI, 6MI, 6MAP, and DMAP are incorporated into oligonucleotides using an automated DNA synthesizer following standard techniques (2). During the process of synthesis and purification no special treatment was given to the probe-containing oligonucleotides.

#### *Guanosine Analog-Containing Oligonucleotides*

The first fluorescence evaluation of pteridine nucleoside analog-containing oligonucleotides was done on the series of 3MI-containing oligonucleotides (listed in Table 2) in which 3MI was substituted for guanosine at various sites (1). Quantum yields listed in Table 2 show that incorporation of 3MI into an oligonucleotide substantially quenches its fluorescence intensity (as compared to the 0.88 of the monomer form). Fluorescence is maximally

quenched when the fluorophore is next to purines and least quenched when next to pyrimidines.

Hawkins and others (1) compared the fluorescence properties of 3MI and 6MI in oligonucleotides representing two different environments, PTER8 and PTER9 (sequences shown in Table 2). Results, presented in Table 3, suggest that 6MI is subject to the same quenching patterns as 3MI, exhibiting substantial quenching when inserted into a purine rich segment of the oligonucleotide (PTER8) but much less quench when inserted into a pyrimidine rich segment (PTER9). In annealing studies of 3MI- and 6MI-containing strands (pairing these two guanosine analogs to cytidine in the opposite strand) quenching for either 3MI or 6MI is not substantially increased upon annealing. This suggests that most of the quenching originates in base stacking rather than base pairing interactions. For PTER 8, the fluorescence signal is very severely quenched (96%) in the single strand for each, 3MI and 6MI, and no additional quench is detected upon annealing. For PTER 9 containing 6MI, quench increases from 56% to 64% with annealing, and for PTER 9 containing 3MI, there is a smaller increase in quench (from 64% to 68%) when the labeled strand is annealed to its complement. The greater quenching effects seen with 6MI upon annealing, suggest that 6MI is more involved in base pairing than 3MI.

In the same study, Hawkins and others (1) found that the emission spectrum of 6MI shifts 7 nm to the red for the probe incorporated into a double strand as compared to unincorporated monomer 6MI. The emission spectrum of 3MI incorporated into a double strand revealed a red shift of 2 nm as compared with the emission spectrum of the 3MI monomer.

Lifetimes, mean lifetimes, and amplitudes for 3MI and 6MI incorporated into single and double strands are shown in Table 3. In the monomer form, the dominant component of the intensity decay curve for 3MI and 6MI has a lifetime of 6.58 ns and 6.26 ns, respectively, but when each of these two fluorophores are incorporated into an oligonucleotide, decay

curves become more complex with shorter lifetime components becoming more prominent. Formation of a double-strand in the highly quenched environment of PTER8 increases the complexity even further for both 3MI and 6MI. In the less quenched environment of PTER9 there is no measurable increase in the complexity of the decay curve and no substantial change in  $\langle\tau\rangle$  in the double strand for 3MI, however the decay complexity for 6MI increases dramatically under the same conditions (Table 3). Based on these data and on the  $T_m$  measurements described below, 6MI appears to participate in base pairing interactions, while 3MI does not. Given the structural features of 3MI, we would expect it to participate little in base pairing interactions. This may in part explain the differences in the observed changes in fluorescence properties of 3MI- and 6MI-containing oligonucleotides.

Disproportionate changes in quantum yield and  $\langle\tau\rangle$  suggest that quenching of 3MI and 6MI is because of a combination of static and dynamic events. Pure dynamic quench is associated with proportional changes in quantum yield and  $\langle\tau\rangle$  while static quench should not be accompanied by a change in  $\langle\tau\rangle$ . The tertiary structure of the oligonucleotide may expose the fluorophore to collisional events from its surroundings (dynamic quenching) or it could position the fluorophore in contact with other bases or backbone quenchers within the oligonucleotide (static quenching). In the 3MI-containing PTER8 single-stranded oligonucleotide, the fluorophore is surrounded by purine bases and the  $Q_{rel}$  is 96% quenched compared with the monomer but the  $\langle\tau\rangle$  of 3MI changes only 30% (6.51 ns to 4.54 ns) under the same conditions (1). This suggests that static quench arising from the surrounding purines is the primary (but not the only) quenching mechanism.

Hawkins and others (1) showed that a pH titration of the emission spectra and DAS of 3MI and 6MI yielded a shift in the emission spectrum of 6MI between pH's 7.0 to 8.0 and an increase in one of 6MI's lifetime components over the pH range from 7.0 to 9.0. These

Table 3  
Fluorescence properties of 3MI (probe 4) and 6MI (probe 17)  
in single and double strands (1).

Probe	PTER		Q% <sup>a</sup>	$\tau_i$ <sup>b</sup> (ns)	$\alpha_1$ <sup>c</sup>	%I <sub>1</sub> <sup>d</sup>	$\tau_m$ <sup>e</sup>
3MI	8	ss	96	$\tau_1=2.35$ $\tau_2=6.06$	$\alpha_1=0.41$ $\alpha_2=0.59$	I <sub>1</sub> =21.2 I <sub>2</sub> =78.8	5.27
3MI	8	ds	96	$\tau_1=0.21$ $\tau_2=2.88$ $\tau_3=6.35$	$\alpha_1=0.70$ $\alpha_2=0.16$ $\alpha_3=0.13$	I <sub>1</sub> =10.0 I <sub>2</sub> =32.5 I <sub>3</sub> =57.5	4.60
3MI	9	ss	64	$\tau_1=2.54$ $\tau_2=5.22$	$\alpha_1=0.31$ $\alpha_2=0.69$	I <sub>1</sub> =17.8 I <sub>2</sub> =82.2	4.74
3MI	9	ds	68	$\tau_1=1.86$ $\tau_2=5.31$	$\alpha_1=0.33$ $\alpha_2=0.67$	I <sub>1</sub> =14.5 I <sub>2</sub> =85.4	4.81
6MI	8	ss	96	$\tau_1=0.30$ $\tau_2=2.21$ $\tau_3=7.28$	$\alpha_1=0.81$ $\alpha_2=0.14$ $\alpha_3=0.06$	I <sub>1</sub> =25.6 I <sub>2</sub> =31.3 I <sub>3</sub> =43.1	3.90
6MI	8	ds	—	$\tau_1=0.21$ $\tau_2=1.20$ $\tau_3=5.89$	$\alpha_1=0.83$ $\alpha_2=0.13$ $\alpha_3=0.03$	I <sub>1</sub> =33.0 I <sub>2</sub> =30.4 I <sub>3</sub> =36.6	2.59
6MI	9	ss	56	$\tau_1=3.45$ $\tau_2=7.01$	$\alpha_1=0.25$ $\alpha_2=0.75$	I <sub>1</sub> =14.1 I <sub>2</sub> =85.9	6.51
6MI	9	ds	64	$\tau_1=0.26$ $\tau_2=1.04$ $\tau_3=6.30$	$\alpha_1=0.88$ $\alpha_2=0.09$ $\alpha_3=0.03$	I <sub>1</sub> =43.4 I <sub>2</sub> =17.0 I <sub>3</sub> =39.6	2.79

<sup>a</sup>% quench relative to the fluorescence of the monomer; <sup>b</sup>lifetime for each component of a multi-exponential model; <sup>c</sup>pre-exponential for each component of a multi-exponential model; <sup>d</sup>% fluorescence intensity for each component of a multi-exponential model; <sup>e</sup>species-concentration-weighted lifetime.

DAS provide a clear signature of an excited state reaction. For 3MI, a shift in the emission spectrum similar to that of 6MI was not seen. This suggests that there is a protonation at the 3-position which is protected by the methyl group in 3MI. A minimum of 2 emitting species (e. g. tautomers) would be needed to explain these DAS.

### Adenosine Analog-Containing Oligonucleotides

In an analysis of 6MAP and DMAP it was found that the fluorescence properties of these probes follow similar patterns to those of 3MI and 6MI. Lifetimes, mean lifetimes, and amplitudes for 6MAP and DMAP incorporated into

single strands are listed in Table 4 (see Table 5 for sequences) (M. Hawkins, et al. submitted). The monomer forms of 6MAP and DMAP display mono-exponential decay with lifetimes of 3.8 and 4.8 ns, respectively, but when these fluorophores are incorporated into an oligonucleotide, decay curves become more complex with shorter lifetime components of the decay curve becoming more prominent. Because of the small variation in the range of Q<sub>rel</sub>'s for oligonucleotides containing 6MAP or DMAP, it is difficult to determine a pattern of fluorescence quenching. (Table 5) The Q<sub>rel</sub>'s for 3MI-containing oligonucleotide ranged from 0.04 to 0.29 (Table 2), while the range for 6MAP-containing oligonucleotides (PTR28, Table 5) was <0.01 to 0.04, and for DMAP-containing

Table 4  
Fluorescence properties of 6MAP and DMAP single strands (Hawkins, M., Pfleiderer, W., Jungmann, O., and Balis, F., submitted).

<sup>a</sup> Oligonucleotides containing 6MAP						
	<sup>b</sup> Q <sub>rel</sub>	<sup>c</sup> τ <sub>i</sub> (ns)	<sup>d</sup> α <sub>1</sub>	<sup>e</sup> %I	<sup>f</sup> τ <sub>m</sub> (ns)	<sup>g</sup> <τ>(ns)
PTR21	0.01	τ <sub>1</sub> =0.69 τ <sub>2</sub> =2.78	α <sub>1</sub> =0.30 α <sub>2</sub> =0.70	9.6 90.4	2.58	2.15
PTR25	0.01	τ <sub>1</sub> =2.93				
PTR27		τ <sub>1</sub> =0.29 τ <sub>2</sub> =1.54 τ <sub>3</sub> =4.73	α <sub>1</sub> =0.40 α <sub>2</sub> =0.53 α <sub>3</sub> =0.07	9.2 64.6 26.2	2.26	1.26
PTR28	0.041	τ <sub>1</sub> =0.17 τ <sub>2</sub> =1.15 τ <sub>3</sub> =2.56	α <sub>1</sub> =0.38 α <sub>2</sub> =0.40 α <sub>3</sub> =0.22	5.9 42.3 51.8	1.82	1.09
HP21	0.01	τ <sub>1</sub> =0.69 τ <sub>2</sub> =3.18	α <sub>1</sub> =0.41 α <sub>2</sub> =0.59	13.1 86.9	2.85	2.16
HP22	>0.01	τ <sub>1</sub> =0.61 τ <sub>2</sub> =3.12	α <sub>1</sub> =0.52 α <sub>2</sub> =0.48	17.5 82.5	2.68	1.81
HP23	0.01	τ <sub>1</sub> =0.48 τ <sub>2</sub> =2.58	α <sub>1</sub> =0.59 α <sub>2</sub> =0.41	21.1 78.9	2.13	1.34
<sup>a</sup> Oligonucleotides containing 6MAP						
PTR32	0.02	τ <sub>1</sub> =0.40 τ <sub>2</sub> =2.90	α <sub>1</sub> =0.39 α <sub>2</sub> =0.61	8.1 91.9	2.7	1.92
PTR38	0.11	τ <sub>1</sub> =0.77 τ <sub>2</sub> =2.80	α <sub>1</sub> =0.42 α <sub>2</sub> =0.58	16.6 83.4	2.46	1.95
HP33	0.02	τ <sub>1</sub> =0.28 τ <sub>2</sub> =2.52	α <sub>1</sub> =0.65 α <sub>2</sub> =0.35	17.1 82.9	2.14	1.06

<sup>a</sup>See Table 5 for sequences; <sup>b</sup>relative quantum yield; <sup>c</sup>lifetime for each component of a multi-component model; <sup>d</sup>pre-exponential for each component of a multi-exponential model; <sup>e</sup>percentage fluorescence intensity for each component of a multi-exponential model; <sup>f</sup>intensity-weighted-lifetime; <sup>g</sup>species-concentration-weighted lifetime.

oligonucleotides (PTR28, Table 5) was <0.01 to 0.11. It is interesting that the two adenosine analogs are so much more severely quenched within an oligonucleotide than the two guanosine analogs. The two highest quantum yields are shown by PTR28 for 6MAP(0.04) and PTR38(0.11) for DMAP (identical sequences) in which the probe is surrounded by pyrimidines. Quantum yields of HP22 and HP32 (identical strands with 6MAP and DMAP respectively) are much lower than one would expect if the

purine/pyrimidine trend was followed.(both are <0.01) Because these are such small numbers, it is important not to over interpret them. Many other factors may impact the quench of these probes in an oligonucleotide. It is interesting that the overall sequence and positioning of the probes in the HP21-24 and HP31-34 series is the same and, regardless of the immediate neighboring base identity, they are all very quenched. DAS for 6MAP- or DMAP-containing double strands have not been exam-

Table 5  
Oligonucleotides containing 6MAP or DMAP at position of F.  
6MAP-containing strands are numbered 21–29 and  
DMAP-containing strands are numbered 31–39. (Hawkins, M.,  
Pfleiderer, W., Jungmann, O., and Balis, F., submitted)

Sequence (5'→3')	w/6MAP <sup>a</sup> (Q <sub>rel</sub> )	w/DMAP(Q <sub>rel</sub> )
gtgtggFaaatctctagcagt	PTR21(0.01)	PTR31(0.02)
gtgtggaaaFtctctagcagt	PTR22(0.02)	PTR32(0.02)
gtgtggaaaatctcFtagcagt	PTR23(0.01)	PTR33(0.01)
actgctFgagattttccacac	PTR24 <sup>b</sup> (0.01)	PTR34(0.01)
actgctagFgattttccacac	PTR25(0.01)	PTR35(0.02)
actgctagagFttttccacac	PTR26(nd)	PTR36(0.02)
actgctagagattttccFcac	PTR27(nd)	PTR37(0.11)
actgctagccFttttccacac	PTR28(0.04)	PTR38(0.11)
attccacaaFgcccgtgtca	HP21(0.01)	PTR31(0.02)
agaggtgtccFctgtggaga	HP22(<0.01)	HP32(<0.01)
agaggtgtacFctgtggaga	HP23(<0.01)	HP33(0.02)
agaggtgtaaFaatgtggaga	HP24(<0.01)	HP34(<0.01)

<sup>a</sup>Relative quantum yields (Q<sub>rel</sub>) are listed in the parentheses; <sup>b</sup>nd means not done.

Table 6  
Oligonucleotides containing 6MAP (Mukerji, I., et al., unpublished).

Name	Sequence <sup>a</sup>	<sup>a</sup> Q <sub>rel</sub> (SS) <sup>2</sup>	Q <sub>rel</sub> (duplex) <sup>b</sup>
A3-1	5' -CGCAFATTTTCGC-3'	0.071	0.053
A3-2	5' -CGCAAFTTTTCGC-3'	0.153	0.081
T3-1	5' -CGCTTTAFACGC-3'	0.093	0.049
AT-1	5' -CGCATFTATCGC-3'	0.164	0.021

<sup>a</sup>F denotes the position of the fluorophore in the oligonucleotide strand. For control sequences F=A.

<sup>b</sup>Quantum yields are relative to the 6MAP monomer.

ined. A comparison of Q<sub>rel</sub>'s of single and double 6MAP-containing strands is listed in Table 6 (I. Mukerji, et al. unpublished). Note that these numbers are somewhat higher than those reported in Table 5 because they are calculated relative to the monomer 6MAP instead of quinine sulfate as a standard. This data (Table 6) describes an increase in quenching upon double strand formation similar to that seen with 3MI and 6MI.

## MELTING TEMPERATURES

T<sub>m</sub>'s have been measured for oligonucleotides containing each of the four pteridine probes, 3MI, 6MI, 6MAP, and DMAP. In Hawkins et al. (1) melting temperatures of the series of 3MI- and 6MI-containing oligonucleotides (shown in Table 2) show that 3MI-containing oligonucleotides display a T<sub>m</sub> depression approximately equivalent to that of

Table 7  
Melting Temperatures of pteridine adenosine analog-containing oligo's  
(Hawkins, M., Pfeleiderer, W., Jungmann, O., and Balis, F., submitted)

<sup>a</sup> Oligo w/6MAP	T <sub>m</sub> (°C)	Oligo w/DMAP	T <sub>m</sub> (°C)
PTR21	56.1°	PTR31	52.4°
PTR22	53.5°	PTR32	51.8°
PTR23	54.8°	PTR33	53.8°
PTR24	57.2°	PTR34	54.6°
PTR25	55.3°	PTR35	57.0°
		PTR36	51.6°
		PTR37	51.0°
Control	57.8°	Control	57.8°

Table 8  
A analog annealing potential different bases (Hawkins, M.,  
Pfeleiderer, W., Jungmann, O., and Balis, F., submitted)

	Base complementary to pteridine analog			
	T	A	C	G
<sup>a</sup> PTR22 (6MAP)	<sup>b</sup> 53.5	43.8	42.8	45.2
PTR32 (DMAP)	51.8	45.2	45.6	46.8

<sup>a</sup>See Table 5 for sequences; <sup>b</sup>(T<sub>m</sub>°C)

a single base pair mismatch. The T<sub>m</sub>'s of double-stranded 6MI-containing oligonucleotides are very similar to the T<sub>m</sub>'s of the controls, however, suggesting that 6MI may participate in base-pairing (1).

Melting temperatures of 6MAP and DMAP-containing oligonucleotides with the adenosine analogs paired to thymidine are shown in Table 7 (M. Hawkins, et al. submitted). As one would expect from the structures, T<sub>m</sub>'s for 6MAP are more similar to those of controls (not containing fluorophores) than DMAP, however, in either case these two probes appear to be quite compatible with double strand formation. In an experiment designed to further characterize the impact of 6MAP and DMAP in a double strand, each was incorporated into the same sequence, paired with the different native bases and evaluated. It is clear from the results in Table 8, that

even though both probes show some destabilization compared to the control, they each are more stable when paired with thymidine than with any of the other three bases.

### P1 NUCLEASE DIGESTION OF 6MAP OR DMAP-CONTAINING SINGLE STRANDS

P1 nuclease digestion of probe-containing single strands serves as a way to determine if quenching of a probe within an oligonucleotide is a function of incorporation into a strand, or from degradation of the probe during DNA synthesis. By digesting separate strands containing either 6MAP or DMAP, we were able to recover the expected fluorescence intensity of the monomer form of each probe. (M Hawkins,

et al. submitted) In order to determine this we measured the fluorescence intensity of a single strand containing one of the probes before and after complete digestion by P1 nuclease. Digestions were done at 37°C overnight. The increase in fluorescence intensity caused by the P1 nuclease digestion was then compared to the difference in relative quantum yields between the single strand containing the probe and the monomer form of the same probe. The results revealed that the fluorescence intensity of these probes is fully recoverable upon digestion. The experiment was done on one strand containing 6MAP (PTR25,  $Q_{rel}$  0.011) and two separate strands for DMAP (PTR35,  $Q_{rel}$  0.02 and PTR37,  $Q_{rel}$  0.11). In each case the fluorescence intensity increase was as expected for full recovery of the monomer form. We have also done this experiment with 3MI and 6MI with similar results. (M Hawkins, et al. submitted)

## SUMMARY OF FLUORESCENCE PROPERTIES

All four of the pteridine probes, 3MI, 6MI, 6MAP, and DMAP, are quite blue with excitation maxima ranging from 310 to 348 nm and emission maxima ranging from 430 to 431 nm. Of the two guanosine analog probes, 3MI has the highest quantum yield (0.88 for 3MI compared to 0.70 for 6MI) and between the two adenosine analogs, DMAP ( $Q_{rel}$  = 0.48) is slightly brighter than 6MAP ( $Q_{rel}$  = 0.39). The effects of incorporation into an oligonucleotide are quite similar for all four probes, although the guanosine analogs do not appear to be as heavily quenched as the adenosine analogs. In each of the four probes, the quench of fluorescence caused by incorporation into an oligonucleotide is fully reversed through digestion of the single strand with P1 nuclease, a strong indication that these probes do not undergo measurable degradation during DNA synthesis and purification. The recoverability of the fluorescence intensity is also an indication of the value of each of these probes for monitoring events that affect the

tertiary structure of DNA. If a probe-containing strand is bent or cleaved in the process of an interaction, the potential increase in fluorescence intensity is considerable. If, for example, a 3MI containing strand has a  $Q_{rel}$  > .02, then a complete digestion of that strand has the potential for an increase of approximately 45 fold as 3MI is completely removed from base interactions.

Evidence from measurement of  $T_m$ 's suggest that 6MI and 6MAP are the most native-like in double strand formation. 3MI, because of the 3-position methyl group would not be expected to anneal very efficiently and the evidence supports this assumption. 3MI is, however, no more destabilizing than a single base pair mismatch.  $T_m$ 's of DMAP-containing strands are slightly more depressed than those of 6MAP-containing strands but the double strands are still somewhat less perturbed than a single base pair mismatch in the same position.

In terms of stability, 3MI appears to be the most unaffected by continuous exposure to the excitation maximum. 3MI was tested in time-based acquisition experiments under exposure to 350 nm excitation for 2 hours at 37°C, without a detectable loss of fluorescence intensity (2). 6MI, 6MAP and DMAP all display a very slow rate of degradation (evidenced by a loss of fluorescence intensity) under time-based acquisition at excitation maxima. Because this loss of fluorescence is only observed during exposure to the excitation maximum in each case, it can be minimized by scanning at intervals to minimize the exposure. All four of the probes show no detectable loss in fluorescence intensity during the course of five successive emission scans. (M Hawkins, et al. unpublished)

The interpretation of the lifetime, quenching and intensity data must take into account the fact that the probe (in a given oligonucleotide environment) may not be homogeneous with respect to position. Some of the changes that we see may be due to unusual orientation in only a small fraction of the probe-containing oligonucleotide especially if that small fraction has a relatively higher fluorescence intensity. This is a

problem shared by all fluorescent probes. In interpretation of steady state data, one must always be aware of the possibility that the changes being recorded may be coming from a subpopulation of probe. One way to avoid this ambiguity is to use time resolved techniques.

From the fluorescence characteristics of these four probes one can envision a number of ways to take advantage of their unique characteristics to monitor structural changes in DNA. In the following pages, we will describe applications that utilize these highly fluorescent analogs in ways that take advantage of the fluorescence properties we have defined.

## APPLICATIONS USING PTERIDINES

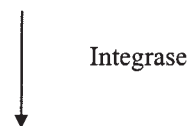
### *HIV-1 Integrase Assay*

A very simple and direct way to take advantage of the incorporated pteridine nucleoside analogs is to monitor changes in fluorescence intensity that occur in response to changes in oligonucleotide structure. An assay was designed to monitor endonucleolytic cleavage activity of integrase protein from HIV-1 using this property (2).

The retrovirally-encoded HIV-1 integrase is a multi-functional protein responsible for the integration of viral DNA into the host cell's genome (7,8). The first step of the mechanism is cleavage of a specific dinucleotide from the 3'-ends of the long terminal repeat (LTR) sequence at either end of the double stranded DNA provirus (3'-processing reaction). Cleavage is followed by other steps, resulting in the integration of the HIV-1 genome into the host cell's DNA. The pteridine-based assay focuses on the cleavage step of this reaction.

The integrase catalyzed 3'-processing and strand transfer reactions have previously been studied *in vitro* using recombinant protein and short double-stranded oligonucleotides (21-mers) with sequences identical to either the U5 or U3 terminus of HIV-1 DNA, as model substrates (9–12). In the real time pteridine-based assay, 3MI, is site-specifically inserted into the

GTGTGGAAAATCTCTAGCAFT - 3'  
CACACCTTTTAGAGATCGTCA - 5'



GTGTGGAAAATCTCTAGCA - 3' + FT - 3'  
CACACCTTTTAGAGATCGTCA - 5'

Fig. 3. Integrase 3'-processing reaction with 3MI-containing substrate (substituting for G). The cleavage reaction of integrase releases the 3MI containing 3' terminal dinucleotide from the strand. 3MI is denoted as F. Adapted from ref. 2.

cleavage site of the double-stranded 21-mer U5 substrate. Figure 3 shows a schematic of the integrase cleavage step with release of 3MI (F) from the oligonucleotide which results in an increase in fluorescence intensity that can be monitored in real time (Fig. 4).

The increase in fluorescence intensity was linear for up to 20 minutes. A blank rate (reaction without integrase protein) showed only slight increases for up to two hours under the same conditions. The rate of the increase in fluorescence intensity is proportional to the rate of the integrase 3'-processing reaction. The potential increase in fluorescence intensity generated by the release of the 3MI-containing dinucleotide is illustrated by the marked difference in the fluorescence emission profiles of the 3MI-containing oligonucleotide and the 3MI-containing dinucleotide shown in Figure 5.

The removal of the fluorophore from a single or double-stranded oligonucleotide through the action of any endo- or exo-nuclease may be presumed to be easily monitored through changes in fluorescence intensity as well. This increase has also been observed using other enzymes including P1 nuclease and Exonuclease III (M Hawkins, et al., submitted) (3).

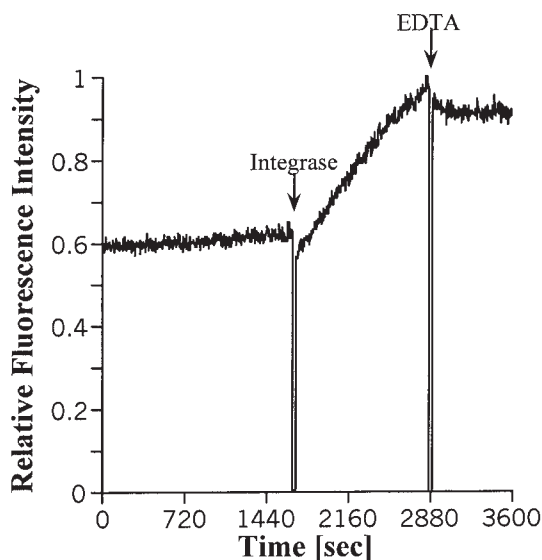


Fig. 4. The real-time kinetic trace of fluorescence intensity depicts the blank rate prior to addition of HIV-1 integrase (0 to 1700 sec), the increase in fluorescence intensity following addition of integrase (1700 to 2880 sec), and cessation of the reaction following the addition of EDTA (>2880 sec) which chelates manganese, a required cofactor. The fluorophore in this substrate is 3MI (Probe 4). Reprinted with permission from ref. 2.

### Alkyl Transferase Coupled Assay

Enzymes that are very selective may not accept substitution of a pteridine for a purine within their active site. In the following assay for the DNA repair protein, O<sup>6</sup> Alkylguanine DNA alkyltransferase (AGT) we describe a way to circumvent this problem by coupling other enzymatic reactions to AGT activity (3). The coupled system allows monitoring of the real time function of AGT within a single reaction mixture.

AGT is one of the more important alkyl transferase proteins responsible for DNA repair (13–15). This protein removes alkyl adducts from DNA consequently counteracting the cytotoxic effect of alkylating agents

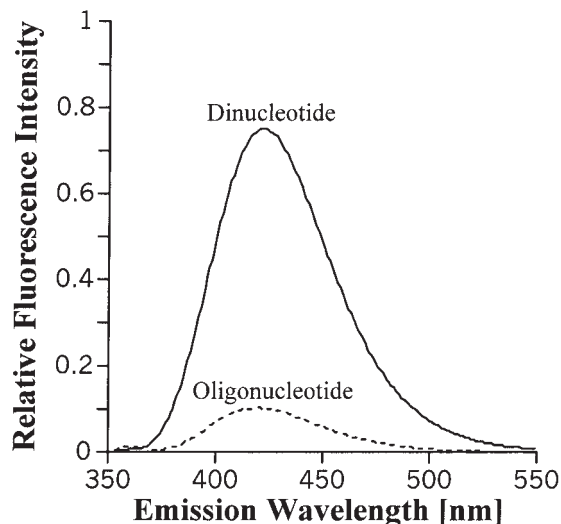


Fig. 5. Comparison of the fluorescence emission spectra for the 3MI-containing substrate oligonucleotide and the 3MI containing dinucleotide cleavage product. 3MI is also Probe 4. Reprinted with permission from ref. 2.

used in cancer chemotherapy. AGT has a highly conserved internal cysteine acceptor site that covalently bonds to alkyl groups attached to the O<sup>6</sup>-position of guanine, irreversibly inactivating the protein. This makes it a good target for inhibitors that would enhance the efficacy of cancer treatment with alkylating agents. The pteridine-based method is an extension of an assay by Wilson and coworkers (16).

In Figure 6, the substrate for the AGT assay is shown with 3MI represented by F and a Pvu II restriction site containing O<sup>6</sup>-methyl guanine (G-Me) in the recognition sequence. The substrate also has a 6 or 7 base overhang on each 3' end. In the coupled series, a restriction endonuclease, Pvu II, will only cleave if and only if AGT first repairs G-Me. In the next step, Exonuclease III (ExoIII) will only significantly digest the substrate after Pvu II cleavage because of its preference for double stranded substrate. Unmodified substrate is protected from Exo III digestion by 3' overhangs designed into the substrate. In the

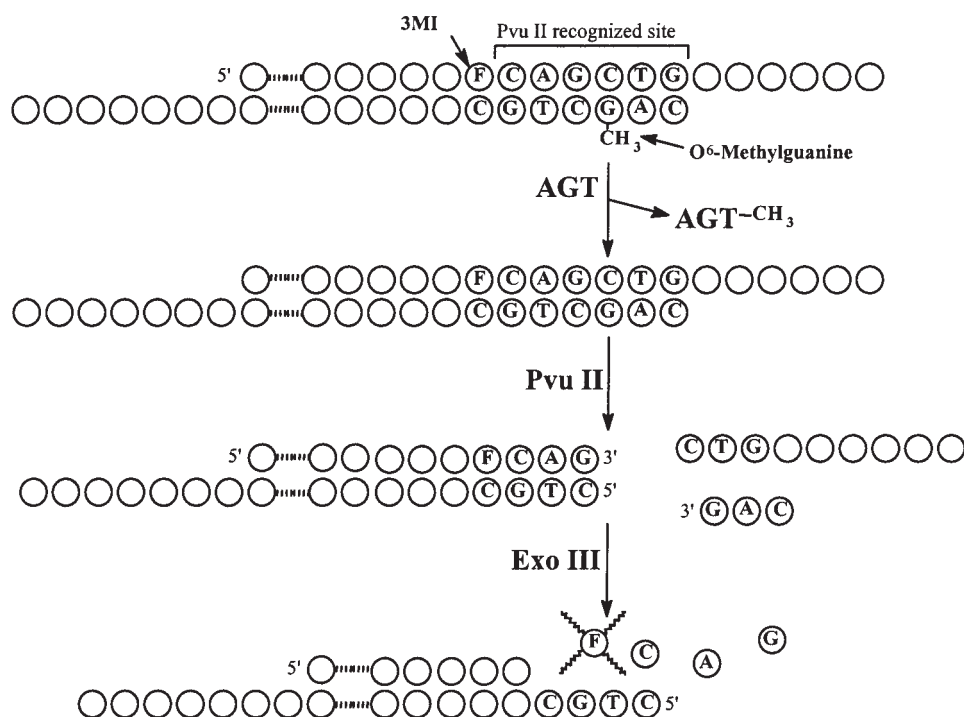


Fig. 6. Fluorescence-based AGT assay sequence. Reprinted with permission from ref. 3.

series, the shorter product of Pvu II cleavage (not containing the fluorophore) dissociates rapidly at 37°C.

This technique is particularly attractive since it allows real time monitoring of AGT activity in a single 100  $\mu$ l volume. Figure 7 shows the blank rate, which is attributed to a possible nickase activity of Exo III along with the AGT rate which has been shown to be proportional to the amount of AGT in the reaction mixture.

We are currently using this assay to study the impact of AGT inhibitors such as O-6 benzyl guanine in cell culture and in patients undergoing treatment with Temazolamide, an alkylating agent. In this study peripheral blood mononuclear cells are isolated from the blood of patients. The cells are then lysed and examined for AGT activity using the assay. By comparing the AGT activity in the cells before and after the patient has received a dose of AGT inhibitor we can determine how effectively the inhibitor is working.

### **Bulge Hybridization Probes**

Hybridization of oligonucleotides containing pteridine nucleoside analogs can be detected in some cases by simply observing the additional quench associated with annealing (2). In order to enhance detection of annealing, however, we have developed the following application. (M. Hawkins and F. Balis, unpublished) Because the quench in fluorescence intensity seen upon incorporation of these probes into oligonucleotides is largely attributable to base stacking interactions, it was reasoned that any disruption in the base stacking arrangement would have a direct influence on the fluorescence intensity. In this application, we explore the effects of forcing a one, two, or three base bulge within a double strand by not providing base pairing partners in the bulge.

The pteridine probe, 3MI, is incorporated into an oligonucleotide that is perfectly complementary to a known target sequence, except for the insertion of the fluorophore. When annealing occurs, the probe is squeezed out of the

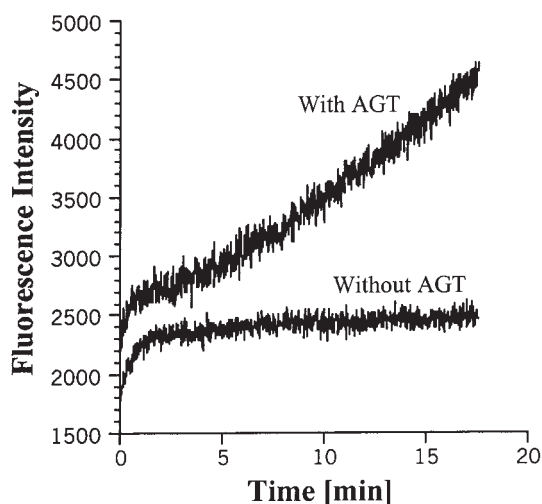


Fig. 7. Real time fluorescence intensity profile of a reaction responding to AGT repair of the methylated substrate shown along with a blank which contains all components of the assay except for AGT. 3MI (Probe 4) is used in the substrate. Reprinted with permission from ref. 3.

strand (it doesn't have a base-pairing partner) partially relieving quench associated with base stacking. This leads to increases in fluorescence intensity up to 27 times the fluorescence of the single strand. Although some increase in fluorescence intensity is seen with 2 or 3 base bulges, the greatest increase is seen with the single base forced out. The degree of increase displayed after annealing the two strands is dependent on the identity of the bases nearest to the fluorophore, (Table 9) with the greatest increases resulting from the pteridine surrounded by adenosines. In this environment the probes are very heavily quenched in a single strand, consequently the background fluorescence (before annealing) is very low.

This highly specific technique may be used to determine the presence or absence of specific DNA sequences in a mixture without the need for separation of annealed or labeled products. Initial studies using 3MI in bulge hybridization to determine the presence of PCR products are very promising. In this application, the probe

strand is designed to bind to the region of product which is between (but not overlapping) the primers. The probe strand is added to the standard PCR mixture before processing in the standard fashion through thermocycling. After amplification, the fluorescence of controls (containing no template) are compared with the fluorescence of reactions containing known amounts of template. Resulting increases in fluorescence are usually between 3 and 4 fold over the blank. (M Hawkins and F Balis, unpublished)

### *Anisotropy Studies on HU Protein*

Studies done at Wesleyan University (2a) have utilized steady state fluorescence anisotropy using 3MI fluorescence to monitor the binding of the HU protein to duplex DNA. HU, a multifunctional histone-like prokaryotic protein, does not bind specifically to a particular sequence of DNA, but does preferentially bind supercoiled and bent DNA. Functioning primarily as an architectural protein similar to HMG, HU facilitates the binding of other proteins to their target sequences by either stabilizing DNA in a bent conformation or possibly inducing a bend upon binding (17).

Fluorescence anisotropy measurements were used to determine the equilibrium binding constants and stoichiometry of HU binding to a 13 bp duplex (H1-13-1) and two 34 bp duplexes (H1-34-1 and H1-34-2) of DNA. The two 34-bp duplexes differ in the placement of the 3MI probe: 5 bases from the 3' end for H1-34-1 and in the middle of the duplex for H1-34-2. Previous studies had suggested that HU binds to 9 bp of duplex DNA; however, stoichiometry experiments performed using either fluorescence anisotropy or analytical ultracentrifugation indicate that 2 HU dimers bind to H1-13-1 and 3 HU dimers bind to H1-34-1 and H1-34-2, respectively. Gel mobility shift assays (GMSA) are indicative of the formation of HU:DNA complexes with stoichiometric ratios of 4 and 5:1 with the 34 bp duplexes. Also, the average apparent binding constants determined by GMSA are 3–4 fold greater than those

Table 9  
Fluorescence increase of bluge forming sequences with 3MI in  
positions marked F (Hawkins, M., and Balis, F., unpublished data)

5 to 3 sequence		
RD9	cttgagccccgaFaactctgactcgg	<sup>a</sup> 20x
HP6	cctctaagaggtgtaaFaatgtggagaatctcc	27x
RD11	agcagt tgctaaagaa Faattgaacacgctcggacttgc	21x
HP4	cctctaagaggtgtaaFagtgtggagaatctcc	14x
RD4	tagacgcttctcaaFaactggaca	12x
PCR2	gcaagatggagaaacaaFggctggagccaa	11x
JS-6	taaataaFaatagtaggtaggctatacattct	9x
RD7	cctgagcgtgagaFaagctggac	8x
JS-5	tgagaaFgagctacacctggccgctcaggcagc	7x
PCR4	attccacaaFgccgtgtca	6x
PCR1	ggctttcgagagFaaccactaccca	5x
RD5	agaagaagataaFagagcgaggcgtcccca	4x
A1Sf-1	ctgcagFaatgggatagagtgcacccagt	3x
RD1	cagaFaaccacaacat	2x
HP5	cctctaagaggtgtccFctgtggagaatctcc	0.3x
HPR	cctctaagaggtgtacFagtgtggagaatctcc	-1.5x

<sup>a</sup>fold increase over single strand

determined by fluorescence anisotropy. The increased affinity of HU in the gel is attributed to the caging effect induced by the medium (18,19). A GMSA was also performed with the 13 bp duplex, however the 13 bp HU-DNA complex undergoes relatively fast dissociation, as detected by smearing in the gel, preventing an accurate determination of an apparent binding constant using this method.

Fluorescence anisotropy assays were performed at a constant concentration of DNA duplex with increasing concentrations of HU protein. As expected, in the absence of HU, the shorter 13-bp duplex has a lower initial anisotropy value relative to the 34 bp duplexes. The H1-34 duplexes exhibit a greater change in anisotropy ( $\Delta r \sim 0.067$ ) upon complex formation than the H1-13-1 duplex ( $\Delta r = 0.033$ ). The binding curves can be analyzed assuming an independent binding site model. Under these conditions the binding constants are well within error of each other with a microscopic  $k$

of  $0.36 \pm 0.09 \mu\text{M}^{-1}$  for the 34 bp duplexes (H1-34-1 and H1-34-2) and  $0.62 \pm 0.16 \mu\text{M}^{-1}$  for the 13 bp duplex (H1-13-1). For H1-13-1, the stepwise binding constants are  $K_1 = 2k$  and  $K_2 = k/2$ , where  $k$  is the microscopic binding constant. Similarly, for the 34 bp duplexes, the stepwise binding constants in terms of the microscopic binding constant are:  $K_1 = 3k$ ,  $K_2 = k$  and  $K_3 = k/3$ . As shown by the fits in Figure 8, the data are well described by this noninteracting binding site model, indicating a lack of cooperativity.

HU exhibits a marked preference for bent DNA and facilitates circularization of DNA (20,21). Upon binding to HU, the 34 bp duplexes, H1-34-1 and H1-34-2 exhibit an increase in fluorescence intensity, which is consistent with increased solvent exposure of the nucleoside analogue. There is a 43% increase in fluorescence intensity upon HU binding to the H1-34-1; in contrast, the fluorescence change for the H1-34-1 duplex is only 23%. This increase in

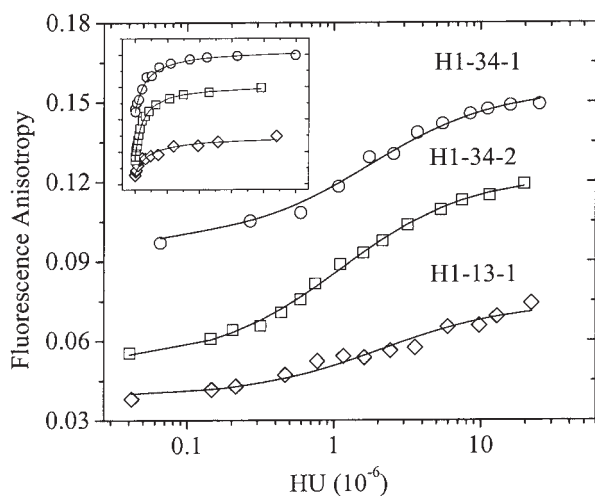


Fig. 8. DNA-binding affinity of HU to 34- and 13-bp duplexes determined by fluorescence anisotropy using 3MI (probe 4). Microscopic binding constants were determined using an independent binding site model, with 3 sites for the 34-bp duplexes and 2 sites for the 13 bp duplex. (O) H1-34-1,  $K_a = 0.24 \mu\text{M}^{-1}$ , for clarity  $r$  shown =  $r$ -values + 0.04;  $\Delta r = 0.067$ . ( $\diamond$ ) H1-13-1,  $K_a = 0.48 \mu\text{M}^{-1}$ ,  $\Delta r = 0.033$ . Inset depicts the same binding curve on a linear scale.

fluorescence intensity is strongly suggestive of a structural deformation of the DNA that leads to an unwinding of the helix and possible unstacking of the DNA bases. The relative difference in the fluorescence intensity change of the H1-34 duplexes upon protein binding is attributed to the degree of quenching caused by the nucleic acid bases adjacent to the 3MI probe. In the H1-34-1 oligonucleotide 3MI is located between two adenosine residues; whereas, in H1-34-2 it is between an adenosine and thymidine. The two flanking adenines in H1-34-1 quench the 3MI fluorescence to a greater extent and because of this relative difference in fluorescence quenching, the H1-34-2 duplex exhibits a greater change in fluorescence intensity upon protein binding. No change in fluorescence intensity is observed upon HU binding to the H1-13-1 duplex.

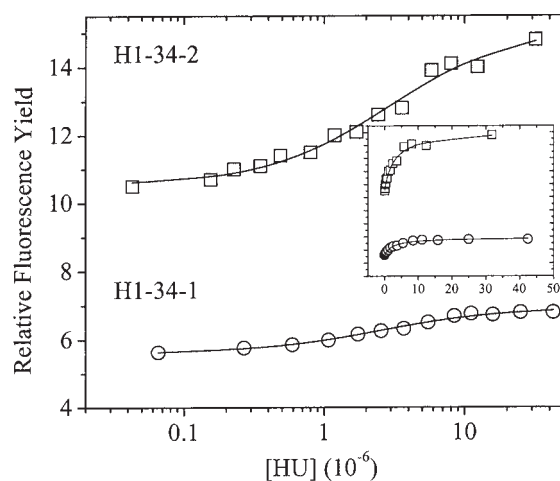


Fig. 9. DNA-binding affinity of HU to 34-bp duplexes determined by fluorescence intensity using 3MI (probe 4). (O) H1-34-1,  $K_a = 0.4 \mu\text{M}^{-1}$ . ( $\square$ ) H1-34-2,  $K_a = 0.34 \mu\text{M}^{-1}$ . Inset depicts the same binding curve on a linear scale.

As shown in Figure 9, the increase in fluorescence intensity as a function of HU concentration exhibits saturable binding, similar to that observed with fluorescence anisotropy. Assuming an independent binding site model, analysis of the curves yields a microscopic  $k$  value of  $0.44 \pm 0.05 \mu\text{M}^{-1}$ , in good agreement with that determined by fluorescence anisotropy. The relative similarity in the binding constants determined for both the intensity and the anisotropy measurements is suggestive of a concerted reaction where HU binding to the DNA is also accompanied by bending.

Mukerji and co-worker's observations reveal that for the 34 bp duplex the number of complexes detected by GMSA is not consistent with the number of complexes observed by fluorescence anisotropy and analytical ultracentrifugation; although the measured binding constants are comparable. In contrast, all three methodologies are indicative of the formation of a 2:1 HU: DNA complex with the 13 bp duplex. The results from the stoichiometry data suggest that the length of the DNA duplex modulates either the size of the binding site or

the mode of binding. In this study the overall 20–40% increase in intensity of 3MI fluorescence upon protein binding to a 34 bp duplex is indicative of decreased base stacking interactions and consistent with a model of induced bending. These results suggest that increased bending upon HU-DNA complex formation may be responsible for the different relative mobilities of the complexes in the gel.

### ***Investigating DNA 'A-Tract' Structure with 6MAP***

The fluorescent adenosine analog, 6MAP has been used to examine the structure of DNA 'A-tracts', which consist of 2 or more adjacent adenine residues. (I. Mukerji, et al. unpublished) When A-tracts are repeated in phase with that of the DNA helix, these sequences exhibit curvature or bending. Gel mobility measurements have revealed that A-tracts of 6 residues exhibit the maximum amount of curvature (22).

6MAP was substituted for an adenine residue in 4 different strands (*see* Table 6). The first two vary the probe position relative to A tracts (A3-1 and A3-2), and the last two are considered to be straight (T3-1 and AT-1). Quantum yields relative to monomer 6MAP from the four oligonucleotide sequences in double and single strands are shown in Table 6. Results reveal that the fluorescence intensity is quenched by ~90% in all four oligonucleotides, relative to free monomer. The adjacent nucleotide neighbors strongly influence the degree of quenching, with maximum quenching observed with the probe surrounded by adenines (A3-1 and T3-1, Table 6) and less quenching with the probe adjacent to pyrimidines (A3-2 and AT-1, Table 6). Incorporation into the single strand does not significantly affect the emission maximum.

Duplex formation further quenches 6MAP fluorescence and follows the same pattern as that seen for 3MI and 6MI by Hawkins, et al (1). The AT-1 oligonucleotide has the highest relative quantum yield as a single-strand and experiences the greatest quench upon duplex formation (87%). In the A3-1 duplex the fluo-

rescence yield is only quenched by 26% relative to the single-stranded oligonucleotide. The absence of a large change in fluorescence yield probably indicates that in the A3-1 oligonucleotide the 6MAP probe stacks well with the adjacent adenine bases, however these interactions are not as strong when the neighboring bases contain at least one pyrimidine. These nearest neighbor interactions are not sufficient to explain the relative quantum yield of the duplexes and undoubtedly, other factors, such as local structure of the duplex, also influence the relative yields. The most striking example of this is the A3-2 duplex, which has one neighboring pyrimidine and the highest fluorescence yield in the duplex, while the AT-1 duplex with two neighboring pyrimidines has the lowest yield.

Duplex formation also leads to a shift in peak emission to shorter wavelengths for all the duplexes studied with 6MAP. The A3-1 and AT-1 duplexes exhibit the largest shifts of –14 and –13 nm, respectively. The emission shift appears to be more reflective of local nucleic acid structure rather than local environment caused by neighboring residues, since the A3-1 and T3-1 duplexes have the same neighboring residues; however, the emission maximum of A3-1 shifts –14 nm while that of T3-1 only shifts –8 nm. Similarly, the A3-2 duplex exhibits the smallest shift in emission maximum, which may reflect the local structure close to the probe. In the case of the A3-2 duplex, the probe position is located at the 3'-end of the A-tract.

Spectroscopic and calorimetric evidence suggests that A-tract duplexes undergo a transition from a bent to a straight conformation and this transition is centered at 35°C. (23–25) This pre-melting transition is characteristic of A-tract duplexes containing an ApT step, such as in A3-1 and A3-2, but is not observed in duplexes containing a TpA step, such as T3-1 (25). In light of our interest in the structure of the above duplexes (Table 6), we have monitored the fluorescence behavior of the single- and double-stranded oligonucleotides as a function of increasing temperature. We observe that the fluorescence intensity of the monomeric probes

and the single-stranded oligonucleotides decrease relatively linearly as a function of temperature. This decrease in intensity is attributed to an increase in the relative efficiency of other processes such as internal conversion and vibrational relaxation. Additionally, increasing the temperature causes a  $-9$  nm shift in peak emission for the 6MAP monomer and an average shift of  $-7.2 \pm 0.9$  nm in emission maximum for the 6MAP single-stranded oligonucleotides. This decrease in peak emission wavelength is attributed to decreased solvent stabilization of the excited state as a consequence of greater thermal motion.

The 6MAP-containing duplexes also exhibit emission maxima shifts as a function of increasing temperature. For all 4 duplexes at  $80^\circ\text{C}$ , the emission maximum shifts to the same value ( $\pm 1$  nm) as that observed for the single-stranded oligonucleotides at  $80^\circ\text{C}$ . This behavior is consistent with exposure of the 6MAP probe to solvent and an absence of stacking interactions at high temperature. The fluorescence intensity of the duplexes can also be monitored as a function of temperature. Since the fluorescence yield of the single-stranded oligonucleotides is greater than that of the duplexes (Table 6), a decrease in fluorescence intensity is observed initially followed by an increase in intensity. A ratio of the fluorescence intensity of the duplex to the single-stranded oligonucleotides yields a sigmoidal curve that is characteristic of the cooperative DNA melting process (Fig. 10). By ratioing the data the decrease in fluorescence intensity as a consequence of increased temperature is suppressed. Similar profiles are obtained if the ratio is done with the monomer and not the single-stranded oligonucleotide. The maximum shift in peak emission occurs at the same temperature as the  $T_m$  from the fluorescence intensity change. Melting temperatures determined from the intensity curves are consistently higher ( $+5$ – $9^\circ\text{C}$ ) than those determined from UV absorption measured at  $260$  nm. Although the source of the discrepancy between the UV and fluorescence data is not clear, it is important to note that the fluorescence data reports on one

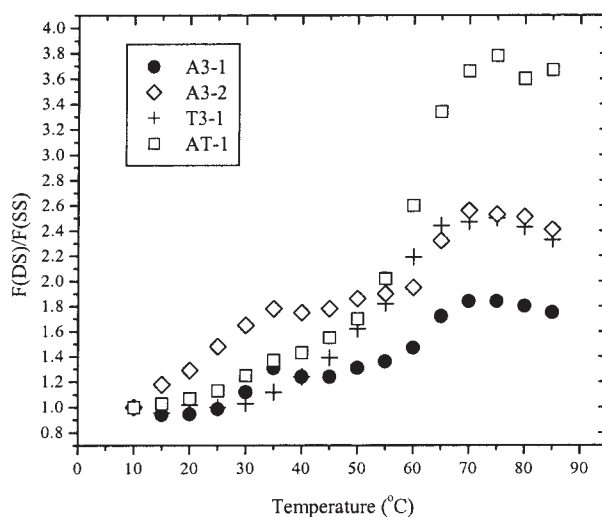


Fig. 10. Fluorescence intensity of the double-stranded 6MAP-containing duplexes relative to the single-stranded oligonucleotides as a function of temperature.

site in the oligonucleotide; whereas, the UV absorption profiles represent an average of all the nucleic acid bases present. In addition, the two techniques are probably reporting on different events in the melting process; specifically, UV absorption reports on the unstacking of the bases and fluorescence profiles monitor both solvent exposure and unstacking. These two events may represent the beginning and end stages of the melting process.

The derivatives of the fluorescence melting profiles (Fig. 11) reveal a clear difference in melting profile between that the A-tract and non-A-tract containing sequences. The melting profile of A3-1 (●) exhibits two distinct maxima representative of two transitions centered at  $30$  and  $62.5^\circ\text{C}$ , while that of AT-1 (□) only has one maximum centered at  $60^\circ\text{C}$ . This premelting transition is also observable in the melting profiles of A3-1 (●) and A3-2 (◇), but not T3-1 (+) duplexes (Fig. 10). The influence of 6MAP on the melting behavior cannot be discounted; however, this influence should also be manifested in the control duplexes T3-1 and AT-1, which show no evidence of a premelting transition. The fluorescence data, which specifi-

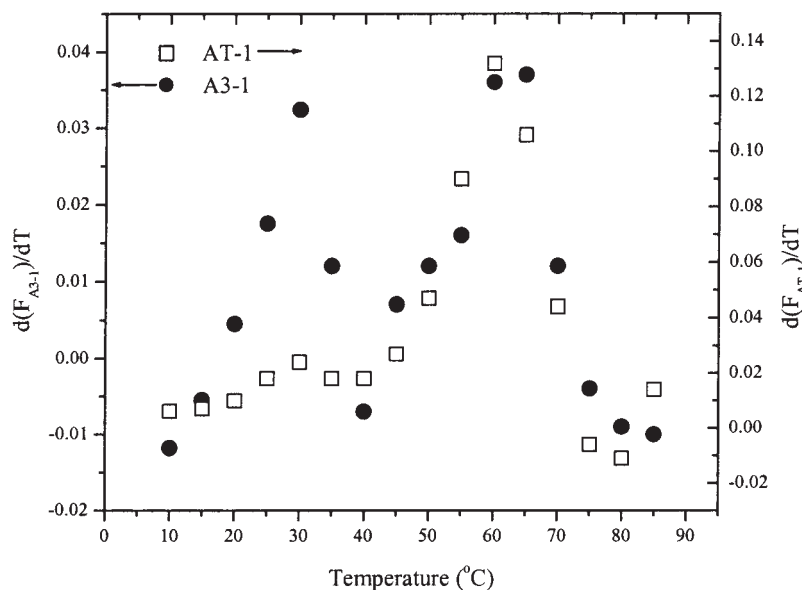


Fig. 11. First derivative of the data shown in figure 10 for 6MAP-containing duplexes. For clarity, only the A3-1 and AT-1 duplexes are shown. A3-1 exhibits two distinct maxima indicative of two transitions at 30 and 62.5°C. AT-1 has one maximum at 60°C.

cally investigates only one site in the DNA duplex, therefore reveals that the locus of the premelting transition is in the A-tract. Furthermore, the highest relative quantum yield is observed for the A3-2 duplex, in which 6MAP is located at the 3' end of the A-tract. This increased fluorescence yield is suggestive of greater solvent exposure of 6MAP in that duplex relative to the other duplexes studied and is consistent with the junction model of bending (22) (Mukerji, I., et al.).

### RNA Polymerase

The utility of 6MI and 3MI as spectroscopic reporters of the interaction of RNA polymerase with both single- and double helical DNA has recently been investigated (W Swingley, M Strainic and P deHaseth, unpublished). The natural target of RNA polymerase is the double stranded promoter DNA, the specific DNA sequence where RNA synthesis is initiated (*see ref. 26*) (26). After the initial contact between RNA polymerase and the double stranded promoter DNA is established, a series of

rearrangements takes place, resulting in the formation of the initiation-competent complex, in which strand separation has occurred over a region of about 14 base pairs which includes the start site of transcription. It is thought that the latter complex, usually referred to as the "open" complex to reflect the strand separation, is stabilized by interactions of the separate single strands with RNA polymerase, rather than with each other. Indeed it has been found that RNA polymerase is able to sequence-specifically interact with stretches of single stranded DNA (27,28).

In prior studies it was demonstrated that the fluorescence of 2-amino purine (2AP), when substituted in the strand-separation region of double stranded promoter DNA, or in single stranded DNA containing certain promoter sequences, was greatly enhanced upon interaction with RNA polymerase (29–31). These results are consistent with an unstacking of the bases in single stranded DNA when it interacts with RNA polymerase. While 2AP substitution has been a useful means to monitor the interaction of DNA with RNA polymerase, there are

Table 10  
Comparison of probes in single strands  
(Swingley, S., Strainic, M., and deHaseth, P.,  
unpublished).

	$k_a \times 10^{-6} \text{ (M}^{-1}\text{s}^{-1}\text{)}$	$k_d \text{ (s}^{-1}\text{)}$
2AP	$0.75 \pm 0.7$	$0.9 \pm 0.1$
3MI	$1.05 \pm 0.02$	$2.24 \pm 0.04$
6MI	$0.56 \pm 0.02$	$1.22 \pm 0.05$

several disadvantages to its use. An important one is 2AP's low quantum yield which necessitates the introduction of two or more substitutions in order to obtain a workable signal at the low DNA concentration dictated by the necessity for maintaining a large excess of RNA polymerase in certain types of experiments. Finally, an obvious limitation is that it could only be used in existing A-T base pairs.

To determine if the 3MI and 6MI base analogs would constitute a suitable alternative to 2AP, first the kinetics of the interaction of RNA polymerase with identical single-stranded 15 mers bearing a 3MI or 6MI at the identical position, or two 2AP at a position with 2 adjacent A-T base pairs, was studied. The fluorescence of the base analogs was monitored at the appropriate wavelengths as a function of time with a stopped flow fluorometer. The oligonucleotides used had the following sequence: 5' AACTATAATTGACTC3'. The substitutions with 3MI or 6MI were at the position of the G; substitution with 2AP was at the two A's at the 5' end. The average results from 3 separate determinations (at 25°C in the buffer as previously used) are displayed in Table 10.

It can be seen that the results with the 3 probes are very similar to each other as well as to previously published results with a longer oligo (31). The errors for the 3MI and 6MI-containing oligonucleotides are smaller than for the oligonucleotide containing 2AP, likely due to the greater signal obtained with the former, despite the fact that they contained only 1 substitution rather than 2 for the 2AP.

The use of 2AP for the study of the kinetics of open complex formation at the *rrnBP1* ribosomal RNA promoter of *E. coli* was problematic, as the region of strand separation is very G-C rich. Here, the use of 6MI was expected to be especially beneficial (note that 3MI does not lend itself to use in double helical DNA as it does not participate in base pairing with C). The partial sequence of the synthetic promoter used for these studies is as follows:

5'-AATTTCTCT**TGACAGGCCGGAATAACTCCC-TATAATGCGCCACCACTGACCTGACAGCGGAA-CAA**-3'

3'-TTTAAAGGAGAACTGTCCGGCCTTATTGAGGG-ATATTACGCFGTGGTACTGGACTGTCGCCTTGTT-5'

Two important RNA polymerase recognition sequences are shown in bold and the region that becomes strand separated in an open complex has been underlined; the start site of RNA synthesis is at the bold A in this region and the 6MI substitution is at the position of the bold E. Upon mixing RNA polymerase (at 12 nM) and 6MI-substituted promoter DNA (at 2nM), a time-dependent increase in 6MI fluorescence is observed, as shown in Figure 12 (average of 10 independent mixing events).

A pseudo first order rate constant of  $0.28 \pm 0.3 \text{ s}^{-1}$  is obtained by fitting the data (red line represents the fit). Applying a two step model for the formation of an open complex to a series of such pseudo first order rate constants collected at various RNA polymerase concentrations, (30,32) an overall rate constant of  $5 \times 10^7 \text{ M}^{-1} \text{ s}^{-1}$  is obtained. This is in good agreement with estimates obtained with a 2AP substituted promoter (substitution at the bold A in the sequence shown above) which gave a marginally useful signal, as well as with determinations by others using manual mixing methods applied to very dilute solutions in order to slow the rate of complex formation. (33)

We conclude that 3MI and 6MI substituted oligonucleotides show great promise as useful agents for monitoring the interaction of RNA polymerase with DNA.

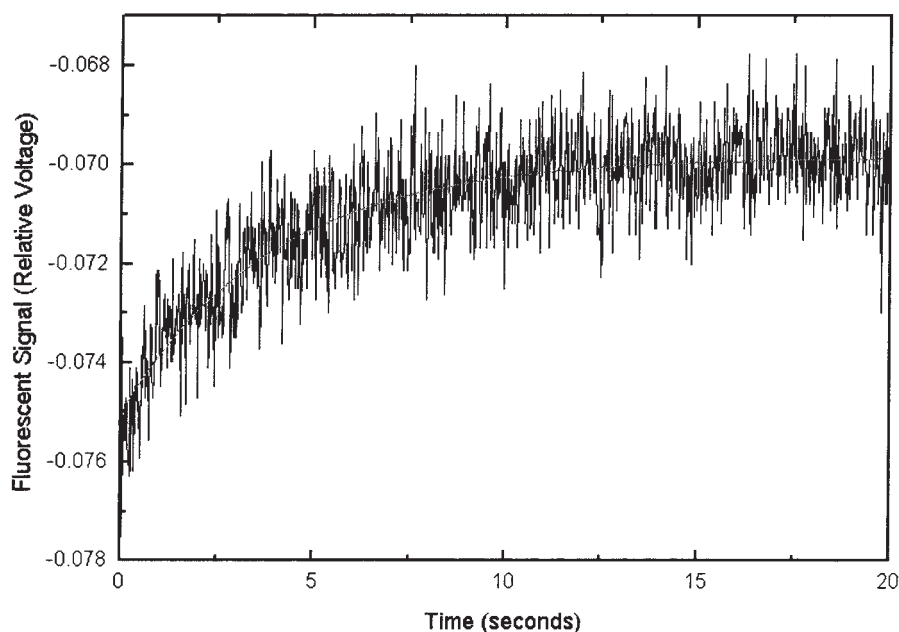


Fig. 12. Time dependent increase in 6MI (Probe 17) fluorescence upon mixing 12nMRNA Polymerase and 2nM 6MI-substituted promoter DNA (Avg of 10 independent mixing events). Note that because of the electronics of the instrument the baseline is negative (Swingley, S., Strainic, M., and deHaseth, P., unpublished).

### ***Intracellular Transport of Oligonucleotides***

The use of pteridine nucleoside analogs for intracellular work is complicated because of high levels of endogenous pteridine fluorescence with excitation and emission properties similar to those of the pteridine probes, resulting in high background fluorescence. One way to overcome this problem is to place multiple probes in a single oligonucleotide in the brightest possible environment (surrounded by pyrimidines in the sequence). This very bright oligonucleotide can then be used to track such things as the fate of therapeutic antisense oligonucleotides.

An example of this approach is given by work at Mt. Sinai in New York by B Hanss and coworkers. (B Hanss, unpublished) The focus of the research is to study the molecular mechanism of oligonucleotide internalization. Overall oligonucleotide uptake by most tissues *in vivo* is relatively low, the highest being

in kidney, liver and brain (34–38). The Hanss group has used isolated perfused renal tubules and an oligonucleotide containing six 3MI molecules as a model to study the kinetics of oligonucleotide uptake in the kidney. For the most part, previous studies on the kinetics of oligonucleotide uptake, have used oligonucleotides end-labeled with either a radioisotope or a fluorescent tag such as fluorescein isothiocyanate (FITC). The rate of uptake for FITC-labeled oligonucleotides appears to be considerably slower than that of radio-labeled oligonucleotides (39). Because of its smaller and less obtrusive structure, 3MI, is being used to explore the source of this discrepancy. Preliminary results have shown that the oligonucleotide (5' -FtccFctcFtctFctcFttcFc-3') containing 3MI at the site of each F, is clearly taken up by isolated perfused renal tubules. A real time visualization of the process using fluorescence microscopy interfaced with digital video capture has shown the rapid uptake of the oligonucleotide. In another experiment,

following discontinuation of the infusion, a delocalization of the brightness revealing the efflux of the 3MI-containing oligonucleotide is clearly apparent (B Hanss, unpublished).

This application demonstrates how the background fluorescence can be overcome by the fluorescence intensity of the 3MI guanosine analog.

## SUMMARY AND OUTLOOK

The ideal probe, one that closely resembles the natural bases and is highly fluorescent, is quite elusive. The characteristics that make guanosine recognizable from the point of view of a protein, for example, are complex and numerous. The size, shape and electron distribution within guanosine all contribute to its being recognized. Nothing can mimic this perfectly without being guanosine and consequently being only faintly fluorescent. Our objective is to create the most native-like, stable and highly fluorescent probes possible. There are substantial differences between fluorescent nucleoside analogs and native nucleosides and yet the similarities in overall shape, size and linkage, allow us to place a fluorophore within the DNA without totally disrupting the tertiary structure. Even though structural studies have not yet been done, we expect the disruption to the DNA is minimal because of the acceptance of the pteridines in the DNA by proteins that require a double stranded substrate.

Using the fluorescent pteridine nucleoside analogs makes it possible to observe subtle changes in DNA by monitoring a variety of fluorescence properties, frequently in a real time format. They provide us with a window on DNA structure and its relationship with its environment.

## ACKNOWLEDGEMENTS

I would like to thank the following people for sharing their research with pteridine

probes in this review: Dr. Ishita Mukerji and Kristi Wojtuszewski at Wesleyan (HU protein); Dr. Basil Hanss at Mt. Sinai (Oligonucleotide Transport); and Wesley Swingley, Michael Strainic and Dr. Pieter deHaseth at Case Western Reserve (RNA polymerase). I also wish to thank Drs. Jay Knutson and Frank Balis for helpful comments and stimulating discussions.

## REFERENCES

1. Hawkins, M. E., Pfeleiderer, W., Balis, F. M., Porter, D. and Knutson, J. R. (1997) Fluorescence Properties of Pteridine Nucleoside Analogs as Monomers and Incorporated into Oligonucleotides. *Analytical Biochemistry* **244**, 86–95.
2. Hawkins, M. E., Pfeleiderer, W., Mazumder, A., Pommier, Y. G., and Balis, F. M. (1995) Incorporation of a Fluorescent Guanosine Analog into Oligonucleotides and Its Application to a Real Time Assay for the HIV-1 Integrase 3'-processing Reaction. *Nucleic Acids Research* **23**, 2872–2880.
- 2a. Wojtuszewski, K., Hawkins, M., Cole, J. L., Mukerji, I. (2001) Hu binding to DNA: evidence for multiple complex formation and DNA bending. *Biochemistry*. **40**, 2588–2598.
3. Moser, A. M., Patel, M., Yoo, H., Balis, F. M., and Hawkins, M. E. (2000) Real-Time Fluorescence Assay for O<sup>6</sup>-Alkylguanine-DNA Alkyltransferase. *Analytical Biochemistry* **281**, 216–222.
4. Stryer, L. and Haugland, R. P. (1967) Energy transfer: a spectroscopic ruler. *Proc. Natl. Acad. Sci.* **58**, 719–726.
5. Driscoll, S. L., Hawkins, M. E., Balis, F. M., Pfeleiderer, W., and Laws, W. R. (1997) Fluorescence Properties of a New Guanosine Analog Incorporated into Small Oligonucleotides. *Biophysical Journal* **73**, 3277–3286.
6. Garcia de la Torre, J. S., Navarro, M. C., Martinez, L., Diaz, F. G., and Cascales, J. J. L. (1994) HYDRO: a computer program for the prediction of hydrodynamic properties of macromolecules. *Biophysical Journal* **14**, 81–139.
7. Esposito, D. and Craigie, R. (1999) HIV integrase structure and function. *Adv Virus Res* **52**, 319–333.
8. Asante-Appiah, E. and Skalka, A. (1999) HIV-1 integrase: structural organization, conformational changes, and catalysis. *Adv. Virus Res.* **52**,

9. Fujiwara, T. and Craigie, R. (1989) Integration of Mini-retroviral DNA: A Cell-free Reaction for Biochemical Analysis of Retroviral Integration. *Proceedings of the National Academy of Sciences* **86**, 3065–3069.
10. Brown, P. O., Bowerman, B., Varmus, H. E., and Bishop, J. M. (1987) Correct Integration of Retroviral DNA In Vitro. *Cell* **49**, 347–356.
11. Brown, P. O., Bowerman, B., Varmus, H. E., and Bishop, J. M. (1989) Retroviral Integration: Structure of the Initial Covalent Product and Its Precursor, and a Role for the Viral IN Protein. *Proceedings of the National Academy of Sciences* **86**, 2525–2529.
12. Vink, C., Banks, M., Bethell, R., and Plasterk, R. H. A. (1994) *Nucleic Acids Research* **22**, 2176–2177.
13. Ellison, K. S., Dogliotti, E., Connors, T. D., Basu, A. K., and M., E. (1989) Site-specific mutagenesis by O<sup>6</sup>-alkylguanines located in the chromosomes of mammalian cells; influence of mammalian O<sup>6</sup>-alkylguanine-DNA alkyltransferase. *Proc. Natl. Acad. Sci.* **86**, 8620–8624.
14. Bogden, P. M., Eastman, A., and Bresnick, E. (1981) A system in mouse liver for the repair of O<sup>6</sup>-methylguanine lesions in methylated DNA. *Nucleic Acids Research* **9**, 3089–3103.
15. Pegg, A. E. et al. (1982) Removal of O<sup>6</sup>-methylguanine from DNA by human liver fractions. *Proc. Natl. Acad. Sci.* **79**, 5162–5165.
16. Wilson, B. D., Strauss, M., Stickells, B. J., Hoalvan Helden, E. G., and Hoalvan Helden, P. D. (1994) An assay for O<sup>6</sup>-alkylguanine-DNA alkyltransferase based on restriction endonuclease inhibition and magnetic bead separation of products. *Carcinogenesis* **15**, 2143–2148.
17. Bewley, C. A., Gronenborn, A. M., and Clore, G. M. (1998) Minor Groove-Binding Architectural Proteins: Structure, Function and DNA Recognition. *Ann. Rev. Biophys. Biomol. Struct.* **27**, 105–131.
18. Fried, M. and Crothers, D. M. (1981) Equilibria and Kinetics of lac repressor-operator interactions by polyacrylamide gel electrophoresis. *Nucl. Acids Res.* **9**, 6505–6525.
19. Fried, M. G. and Liu, G. (1994) Molecular sequestration stabilizes CAP-DNA complexes during polyacrylamide gel electrophoresis. *Nucl. Acids Res.* **22**, 5054–5059.
20. Paull, T., Haykinson, M., and Johnson, R. (1993) The nonspecific DNA-binding and bending proteins HMG1 and HMG2 promote the assembly of complex nucleoprotein structure. *Genes Dev.* **7**, 1521–1534.
21. Hodges-Garcia, Y., Hagerman, P. J., and Pettijohn, D. E. (1989) DNA Ring Closure Mediated by Protein HU. *J. Biol. Chem.* **264**, 14621–14623.
22. Crothers, D. M. and Shakked, Z. *DNA Bending by adenine-thymine tracts* (ed. Neidle, S.) (Oxford University Press, Oxford, 1999).
23. Chan, S. S., Breslauer, K. J., Austin, R. H., and Hogan, M. E. (1993) Thermodynamics and Premelting Conformational Changes of Phased (dA)<sub>5</sub> Tracts. *Biochemistry* **29**, 6161–61171.
24. Chan, S. S., Austin, R. H., Mukerji, I., and Spiro, T. G. (1997) Temperature-Dependent Ultraviolet Resonance Raman Spectroscopy of the Premelting State of dA.dT DNA. *Biophysical Journal* **72**, 1512–1520.
25. Park, Y. W. and Breslaueer, K. J. (1991) A Spectroscopic and Calorimetric Study of the Melting Behaviors of a 'bent' and 'normal' DNA Duplex:[d(GA4T4C)]<sub>2</sub> versus [d(GT4A4C)]<sub>2</sub>. *Proceedings of the National Academy of Sciences* **88**, 1551–1555.
26. deHaseth, P. L., Zupancic, M., and Record Jr., M. T. (1998) RNA polymerase-promoter interaction: the cmings and goings of RNA polymerase. *J. Bacteriol* **180**, 3019–3025.
27. Marr, M. T. and Roberts, J. W. (1997) Promoter recognition as measured by binding of RNA polymerase to nontemplate strand oligonucleotides. *Science* **276**, 1258–1260.
28. Savinkova, L. K. et al. (1993) *Escherichia coli* RNA polymerase interaction with the oligonucleotides homologous to “-10” and “-35” regions of bacterial *spc* promoters. *Mol. Biol.* **27**, 33–37.
29. Sullivan, J. J., Bjornson, K. P., Sowers, L. C., and deHaseth, P. L. (1997) Spectroscopic determination of open complex formation at promoters for *Escherichia coli* RNA polymerase. *Biochemistry* **36**, 8005–8012.
30. Strainic, J., M. G., Sullivan, J. J., Velevis, A., and deHaseth, P. L. (1998) Promoter recognition by *Escherichia coli* RNA polymerase: Effects of the UP element on open complex formation and promoter clearance. *Biochemistry* **37**, 18074–18080.
31. Fedoriw, A. M., Liu, H., Anderson, V. E., and deHaseth, P. L. (1998) Equilibrium and kinetic parameters of the sequence-specific interaction of *Escherichia coli* RNA polymerase with nontemplate strand oligodeoxyribonucleotides. *Biochemistry* **37**, 11971–11979.
32. McClure, W., Hawley, D., and Malan, T. P. (1984) The Mechanism of RNA Polymerase

- Activation on the Lambda PRM and lac P+ promoters.,
33. Rao, L. et al. (1994) Factor independent activation of *rrnB* P1. An "extended" promoter with an upstream element that dramatically increases promoter strength. *J. Mo.. Biol.* **235**, 1421–1435.
  34. Cossum, P. A. et al. (1993) Disposition of the 14C-labeled phosphorothioate oligonucleotide ISIS 2105 after intravenous administration to rats. *J. Pharmacol. Exp. Ther.* **267**, 1181–1190.
  35. Meeker, R., Legrand, G., Ramirez, J., Smith, T., and Shih, Y. H. (1995) Antisense vasopressin oligonucleotides: Uptake, turnover, distribution, toxicity and behavior. *Journal of Neuroendocrinology* **7**, 419–428.
  36. Oberbauer, R., Schreiner, G. F., and Meyer, T. W. (1995) Renal uptake of an 18-mer phosphorothioate oligonucleotide. *Kidney International* **48**, 1226–1232.
  37. Ogawa, S., Brown, H. E., Okano, H. J., and Pfaff, D. W. (1995) Cellular uptake of intracerebrally administered oligodeoxynucleotides in mouse brain. *Regul. Pept.* **59**, 143–149.
  38. Rappaport, J. et al. (1995) Transport of phosphorothioate oligonucleotides in kidney: implications for molecular therapy. *Kidney Internat.* **47**, 1462–1469.
  39. Zhao, Q., Waldschmidt, T., Fisher, E., Herrera, C. J., and Krieg, A. M. (1994) Stage-specific oligonucleotide uptake in murine bone marrow B-Cell precursors. *Blood* **84**, 3660–3666.